GCA TECHNICAL REPORT NO. 62-12-N

67 p.

ON THE QUESTION OF TURBULENCE IN THE UPPER ATMOSPHERE

OWEN COTE

CONTRACT NO. NAS5-215

PREPARED FOR
NATIONAL AERONAUTICS AND SPACE ADMINISTRATION
HEADQUARTERS
WASHINGTON 25, D. C.

OCTOBER 1962

GEOPHYSICS CORPORATION OF AMERICA
BEDFORD, MASSACHUSETTS

(NASA CR- ; GCA Technical Report No. 62-12-N) OTS:

ON THE QUESTION OF TURBULENCE IN THE UPPER ATMOSPHERE

Owen Cote

(NASA Contract No. NAS5-215)

October 1962

GEOPHYSICS CORPORATION OF AMERICA
Bedford, Massachusetts

Prepared for

NATIONAL AERONAUTICS AND SPACE ADMINISTRATION
HEADQUARTERS
WASHINGTON 25, D. C.

ABSTRACT

11298

Photographic sequences of rocket produced sodium vapor trails, illuminated by resonant scattering of twilight solar radiation, are available for fourteen twilights in the period November 1950 to June 1962. The radial expansion of the luminous cloud image for 9 December 1960 (AM) and 17 September 1961 (AM) is reduced to a measure of the transverse horizontal dispersive power of the atmosphere. Turbulence in the region above 112 km is excluded as a mechanism in the horizontal dispersion of the sodium vapor; the radial growth of the cloud at 112 km is explained by molecular diffusion with a diffusion coefficient equal to 6.8×10^6 cm^2/sec.

Below this height evidence in the 100-108 km region indicates an accelerated cloud growth for diffusion times greater than 35 seconds, the variance of the integrated line-of-sight distribution of sodium is proportional to t^2. The association of the accelerated growth of the trail after 35 seconds with pre-existing atmospheric turbulence is unambiguous only if the effect of turbulence created by the wake and in the jet release of the vapor does not accelerate molecular diffusion or interact with and remove energy from the large scale strain field of the atmosphere, and if the large scale divergence in combination with molecular diffusion is too small to account for the measured growth of the trail. The large scale motions which distort the cloud in the 100 to 120 km region have horizontal motions whose vertical variation is of the order of the atmospheric scale height for density. AUTHOR

TABLE OF CONTENTS

SECTION 1

INTRODUCTION

In recent years a series of experiments with artificially generated sodium clouds has been performed by Manring et al.[1] Earlier experiments with sodium clouds and the physical processes involved were reported by Bedinger et al.[2] and Marmo et al.[3] The method of forming the sodium vapor involves the vaporization of pellets of metallic sodium by heat generated from combustion of an iron oxide-aluminum thermite mixture. The vaporizer was a 12" long x 6" diameter cylinder with three 3/4" diameter ejection ports equally spaced around the circumference. The burning time of the mixture, approximately three minutes in flight, was controlled by the size of the sodium pellets, the ratio of sodium to thermite, and the pressure under which the cylinder was homogeneously packed. The vaporizer was fitted to the nose cone of a Nike-Asp rocket, which transits the 90 - 115 km region with a velocity between 1.4 and 1.0 km/sec. Sequences of photographs, of which Figure 1 is typical, record the distortion and radial expansion of the quasi-cylindrical trail. These twilight releases of sodium trails, illuminated by resonant scattering of solar radiation, were specifically performed to yield data on winds and diffusion.

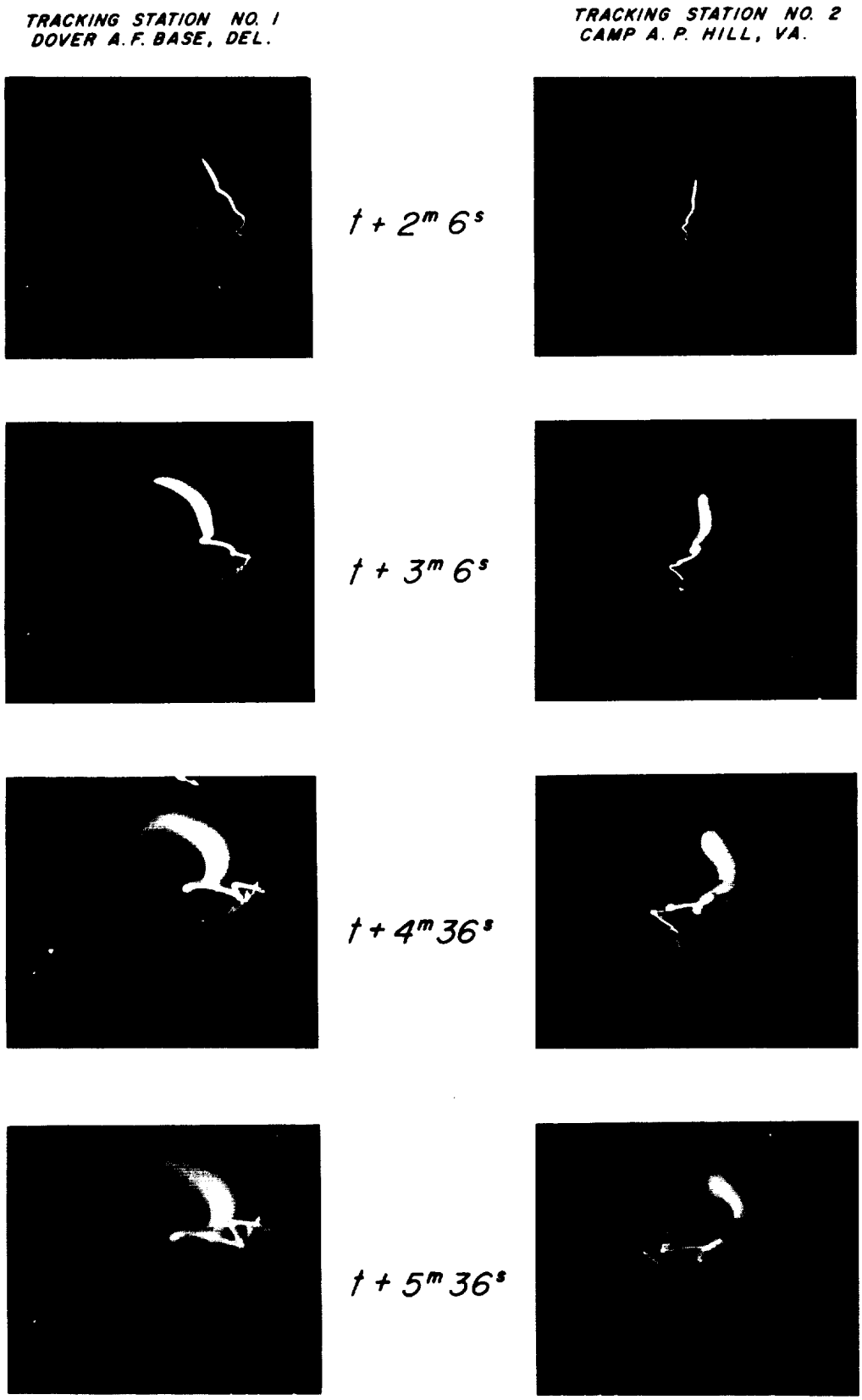

Figure 1. Typical cloud distortions caused by the vertical variations of the horizontal wind.

Diffusion coefficients reported by Manring[4] indicate an agreement between sodium cloud values above 120 km and a standard atmosphere extrapolation from the sea-level value. Below 120 km the values, determined from the sodium clouds, are consistently larger than the extrapolated values. Furthermore, up to a height level, 102±4 km, the up-trail becomes irregular in appearance (see Figure 2) within seconds after the release of the sodium vapor from the rocket. This irregular appearance has also been observed in British and French sodium experiments[5] and seems to characterize all rocket generated sodium trails. Blamont[5] reports a corresponding phenomena in the down-trail at corresponding heights. However, this is not true of the GCA-NASA trails generated at Wallops Island. The question of the existence of turbulence in the 85 to 125 km region is raised by these qualitative observations. To answer this question, we consider the diffusive growth of the sodium trails as the final arbiter.

SECTION 2

THEORIES OF TURBULENT DIFFUSION

The absence of any method of direct sampling of velocity fluctuations suggests consideration of a diffusion-type experiment. This is a simple method for obtaining indirectly information on the existence of a random velocity field which characterizes a fluid in turbulent motion. Turbulent motions are characteristically unstable to small disturbances which may include fluctuations in temperature and density. It is this instability which makes it impossible from a knowledge of initial and boundary conditions to predict the velocity at any given point in space or time. This unpredictability necessitates descriptions by probability distribution functions (p.d.f.). The p.d.f. may be obtained theoretically or empirically from a large number of reproducible experimental trials.

It has been shown by Batchelor[6] in his study of diffusion in a field of homogeneous turbulence that, once the initial shape of a cloud of marked particles is known, its subsequent tendency to change its shape, which is directly related to the possibility of a vector $\underline{y}$ being

completely immersed in the cloud, will be determined by the statistical properties of the separation of two particles. The most meaningful parameter is the second moment of the two particle separation $\langle y_i\ y_j \rangle$. Specific predictions of the form

$$\langle y_i\ y_j \rangle \sim t^{\alpha}$$

have been made, which are based on the various formulations of turbulence theory. Before introducing these predictions, it will be helpful for later interpretation if the problem of relative diffusion is outlined in some generality.

Consider first the simpler single particle analysis. A dynamically passive scaler is used to mark a fluid "particle". Its subsequent history is

$$\underline{x}(t) = \underline{x}_o + \int_{t_o}^{t} \underline{v}(t', \underline{x}_o)dt'$$

where $\underline{v}(t)$ is a lagrangian velocity following the motion which originated at $\underline{x}_o$ at time t_o. An ensemble of such trials will generate the probability distribution function $P(\underline{x},t|\underline{x}_o t_o) = P(\underline{x},t)$. It represents the probability that a particle (or property) initially in the volume $d\underline{x}_o$ about $\underline{x}_o$ at time t_o will be found in the volume $d\underline{x}$ about $\underline{x}$ at a subsequent time t. The reformulation of the lagrangian p.d.f. in terms of Eulerian moments

(Batchelor[6] Roberts[7]) follows as below. Represent the dynamically passive scalar field by $\varphi(\underline{x},t)$ in any one realization. Continuity in this simple convective model requires

$$\frac{\partial}{\partial t}\left(\varphi(\underline{x},t)\right)+\frac{\partial}{\partial x_i}\left(\varphi(\underline{x},t)\ u_i(\underline{x},t)\right)=0$$

$u_i(\underline{x},t)$ is the fluctuating velocity. Molecular diffusion is neglected. For a single particle

$$\varphi(\underline{x},t)=\delta(\underline{x}-\underline{x}_t)$$

where $\underline{x}_t$ is the position at time t of the fluid particle that was at $\underline{x}_o$ at time t_o. The ensemble averaged equation

$$\frac{\partial}{\partial t}\langle\varphi(\underline{x},t)\rangle+\frac{\partial}{\partial x_i}\langle\varphi(\underline{x},t)\ u_i(\underline{x},t)\rangle=0$$

satisfying the initial conditions

$$\langle\varphi(\underline{x},t_o)\rangle=\delta(\underline{x}-\underline{x}_o)$$

has a solution

$$\langle\varphi(\underline{x},t)\rangle=P(\underline{x},t|\,\underline{x}_o,t_o)$$

The probability of finding marked fluid at any point is equivalent to the mean concentration of marked fluid. The complication of an infinite number of dynamic equations that is required to relate the coupled moments follows from the similar but more complicated equations for $\langle \varphi\, u_i \rangle$. Utilizing the momentum equation, the equation for $\frac{\partial}{\partial t} \langle \varphi\, u_i \rangle$ contains higher moments; such as, $\langle u_i\, u_j\, \varphi \rangle$. The coupling of the moments due to the nonlinearity of the defining equations necessitates an infinite set of moment equations for a determinate problem. The closure problem of turbulence theory represents the attempt to reduce the problem to a finite number of equations. (Kraichnan[8]).

A similar closure problem exists when we consider the more complicated case of two particles released into a turbulent fluid. The ensemble of such experiments will generate the joint probability distribution function $Q(\underline{x}', t'; \underline{x}'', t'' | \underline{x}'_o, t'_o; x''_o, t''_o)$. This is the probability that particles which originated at $\underline{x}'_o$ and $\underline{x}''_o$ at t'_o and t''_o, respectively, will have travelled to $\underline{x}'$ and $\underline{x}''$ at t' and t''. By replacing $\underline{x}'$ and $\underline{x}''$ by $\underline{X} = \underline{x}' - \underline{x}'_o$ and $\underline{y} = \underline{x}'' - \underline{x}'$, we may distinguish the translation of the particle pair from their separation. The reformulation of the joint p.d.f. into one involving Eulerian moments follows as in the single particle analysis.

Introduce $\varphi_1(\underline{x}',t')$ as the passive scalar function for the first "particle" and $\varphi_2(\underline{x}'', t'')$ for the second. They satisfy the continuity relation and initial conditions separately:

$$\frac{\partial \varphi_1(\underline{x}',t')}{\partial t'} + \frac{\partial}{\partial x'_i}\left(\varphi_1(\underline{x}',t')\ u_i\ (\underline{x}',t')\right) = 0$$

$$\varphi_1(\underline{x}',t'_o) = \delta(\underline{x}'-\underline{x}'_o)$$

and

$$\frac{\partial \varphi_2(\underline{x}'',t'')}{\partial t''} + \frac{\partial}{\partial x_i''}\left(\varphi_2(\underline{x}'',t'')\ u_i\ (\underline{x}'',t'')\right) = 0$$

$$\varphi_2(\underline{x}'',\ t''_o) = \delta(\underline{x}''-x''_o)$$

A similar closure problem exists for the covariance $\langle\varphi_1(\underline{x}',t')\ \varphi_2(\underline{x}'',t'')\rangle$ which defines the joint p.d.f.

$$Q(\underline{x}',t';\underline{x}'',t'')\,|\,\underline{x}'_o,t'_o;\underline{x}''_o,t''_o) = \langle\varphi_1(\underline{x}',t')\ \varphi_2(\underline{x}'',t'')\rangle$$

(See Roberts[7], Kraichnan[8]).

The most meaningful parameter derivable from the separation p.d.f. is the second integral moment (relative dispersion tensor σ_{ij})

$$\sigma_{ij}(t|\underline{y}_o, t_o) = \langle y_i(t)\ y_j(t)\rangle = \int y_i y_j\, Q(\underline{y}, t|\underline{y}_o t_o)\ d\underline{y}$$

which may be related to the relative velocity of the two particles.

$$\langle y_i(t)\ y_j(t)\rangle = \langle y_i(t_o)\ y_j(t_o)\rangle + \int_{t_o}^{t} dt' \int_{t_o}^{t} dt'' \langle v_i(t')\ v_j(t'')\rangle$$

The relative dispersion tensor σ_{ij} is accessible if we can evaluate the evolution of the joint p.d.f., or the relative velocity covariance $\langle v_i(t')\ v_j(t''\rangle$. Some form of approximate closure of the infinite set of moment equations has been obtained by specific postulates about statistical properties - Kolmogorov's universal equilibrium theory, or about dynamic processes - Heisenberg's eddy-viscosity theory (See Batchelor[9]). Recently Kraichnan has attempted an analytic approximation of closure (Kraichnan[9],[10]). From these various theories of turbulence, theories of turbulent diffusion may be derived which will give specific predictions for the form of the law of relative dispersion. In the appendix of this report, some of these specific predictions are indicated.

SECTION 3

THE SIMILARITY THEORY OF RELATIVE DISPERSION

The idea that some kind of statistical decoupling accompanies the transfer of energy from the large scale to the small scale motions where the small eddies tend to be statistically isotropic was first suggested by Kolmogorov; it was formulated into two similarity hypotheses:[10]

(1) "The statistical properties of the small-scale components of any turbulent motion with large Reynolds numbers are determined uniquely by the quantities ν and ϵ".

ν = kinematic viscosity

ϵ = the average rate of dissipation per unit mass of fluid

(2) "At sufficiently larger Reynolds numbers of the turbulence, there is an inertial subrange in which the average properties are determined uniquely by the quantity ϵ".

One can associate a characteristic length ℓ_o with a range of wave numbers in which most of the energy is contained and u with a characteristic velocity $\frac{1}{3} \langle u_i u_j \rangle^{\frac{1}{2}} = u_o$. If the initial separation vector $\underline{y}_o$ is small in

comparison with the length scale ℓ_o then the universal equilibrium theory may be assumed valid with the following consequences for the separation p.d.f. $Q(\underline{y},t/\underline{y}_o,t_o)$. For large Reynolds numbers $Q(\underline{y},t/\underline{y}_o,t_o)$ becomes an isotropic function of $\underline{y}$, $\underline{y}_o$ and $t-t_o$. The relative dispersion tensor $\langle y_i y_j \rangle$ will also become an isotropic function

$$\langle y_i y_j \rangle = \langle y^2 \rangle \delta_{ij}$$

in which its dependence upon the turbulence will be only through the parameters ν and ϵ. The diffusivity is defined

$$D_{ij} = \tfrac{1}{2} \frac{d}{dt} \langle y_i y_j \rangle$$

and may be evaluated by dimensional arguments. It will be expressed as a universal function of the parameters ν and ϵ, describing the turbulence, and the variables t and $\underline{y}_o$. Batchelor[6][10] gives the following predictions as a consequence of the similarity theory:

For small times $\quad t << y_o^{1/3} \epsilon^{-1/3}$

$$\frac{d}{dt} \langle y^2(t) \rangle = t^2 \epsilon G(y_o/\epsilon^{1/2} t^{3/2})$$

for intermediate times $t >> \ell_o^{2/3} \epsilon^{-1/3}$ (provided $\underline{y}(t)$ is still within the inertial range)

$$\frac{d\langle y^2\rangle}{dt} = \text{const. } \epsilon t^2$$

For large times $t \to \infty$.

$$\frac{d\langle y^2\rangle}{dt} \to 2\,\frac{d\langle X^2\rangle}{dt}$$

where $\langle X^2\rangle$ represents the mean square dispersion for a single particle from a fixed origin.

The time (t_1) which marks the division between the "small" and "intermediate" values of diffusion time t will have a parametric representation

$$t_1 = k\, y_o^{2/3}\, \epsilon^{-1/3}, \quad k = 0(1).$$

Integration of these two predictions gives:

Case I small times

$$\langle y^2(t)\rangle - \langle y^2(o)\rangle \sim t^2\, (\epsilon y_o)^{2/3}$$

Case II intermediate times

$$\langle y^2\rangle \sim \epsilon t^3$$

SECTION 4

OBSERVATIONS

The observational data available are sequences of photographic negatives from five camera sites. Three film and lens combinations are used: 80 mm f/2.8 lens with 70 mm roll film (See Figure 2) and a K-24 aerial camera using 5" x 7" strip film with either 7" f/2.5 (See Figure 4) or 20" f/5.6 lens (See Figure 3). Exposure times used with the 70 mm film were 3, 6, 7 and 12 seconds. The 5" x 7" film exposures are either 6 or 10 seconds. The cameras are electrically controlled and automatic. Exposure sequences are usually not adjusted during the course of a single twilight experiment. The rapid changes in sky brightness that occur are compensated by adjusting the lens openings.

Against the sky background the sodium cloud is illuminated by a resonance scattering process. The cloud image recorded on the negative represents the response of the film and camera optics to the photons emitted by solar illuminated sodium atoms. It is estimated[3] that the absorption cross-section for sodium is 10^{-11} cm^2. Hence, integrated line-of-sight densities greater than 10^{11} atoms/cm^2 will be optically

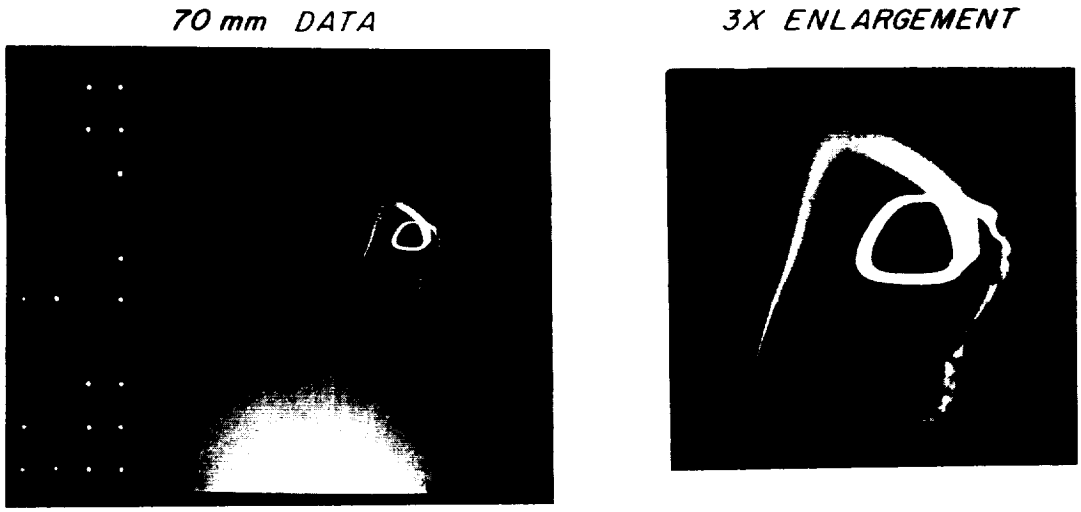

Figure 2. A composite of photographs from three different camera sites. It typifies the kind of data which is available and illustrates the obvious transition in the appearance of the cloud.

110 sec 70 sec 30 sec

20" f/5.6 K-24 camera

Figure 3. Initial cloud growth, from Dam Neck, Va.
17 September 1961 (AM).

(a) 9 December 1960 (AM)

6 min. after rocket launch

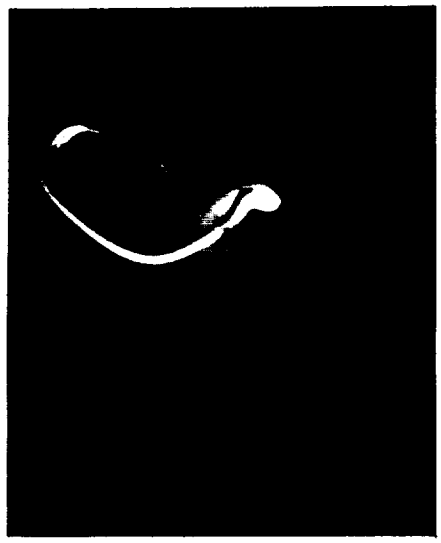

5 min. after rocket launch

Note that the straight region just before loop in the up trail cloud is irregular and the corresponding parallel straight region in down trail is smooth.

(b) 17 September 1961 (AM)

6 min. after rocket launch

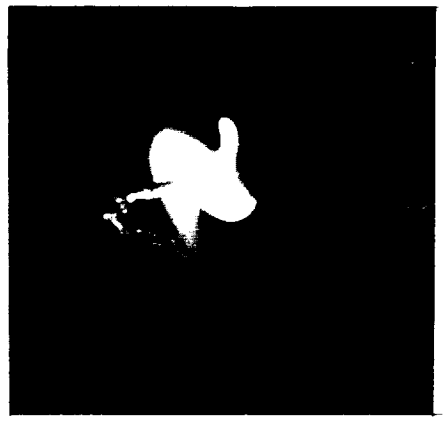

5 min. after rocket launch

Figure 4. View of clouds from Wallops Island rocket launch site. (K-24 7" f/2.5 data)

dense to the solar illumination and will not be represented by correspondingly darker images on the negative. At the edge of the cloud, some minimum line-of-sight concentration will be required to darken the negative sufficient to just make a visible contrast with the background darkening of the negative. Between these two extremes, if the film response characteristics, negative density vs. source intensity x exposure time, are linear, then densitometry of the negative will generate a relative integrated line-of-sight distribution function for the sodium concentration. In principle, the time rate of change of the variance of this distribution will give a measure of the dispersion of the sodium cloud. Practically, the difficulties associated with

(a) the changing viewing angle;

(b) the changing background light intensity;

(c) uncertainties of the film sensitivity;

(d) the changing lens openings; and

(e) the magnitude of the cloud transport during exposure

timesof 6 to 12 seconds interact in such a complex manner that the greater labor involved in densitometry of the negatives was postponed in favor of the more easily measured visible diameter measurements. Instead of a continuous distribution of relative cloud intensity with distance across the cloud, the visible edge represents one relative intensity which corresponds with one diameter measurement for each

successive photograph. As long as a cloud edge is well defined and identifiable in successive photographs, one obtains an objective length measure whose meaning shall presently be explored. These measurements are restricted to the horizontal growth of the cloud diameter, hereafter called "transverse",which is perpendicular to the velocity of cloud transport in those height regions where the phase change of the horizontal velocity vector with height is either zero or suitably small. The azimuth angle of the camera in the outlying sites closely parallels the direction of transport of the cloud or that direction plus 180 degrees. This last restriction is particularly important for camera sites to the north or south of the cloud. The mean west-east transport is ~40 m sec^{-1} which causes a cloud transport ~200 meters during a six-second exposure. With cloud diameters ~100 meters 10 seconds after release, the cloud image diameter is subject to a large overestimation. Toward the end of the photographic sequence when the diameter of the cloud is ~8 km, this factor is much less important.

In seeking to establish the quantitative nature of the diffusivity of the upper atmosphere, there are limitations imposed by the sampling restrictions of the sodium trail dimensions: diffusion time less than 12 minutes and cloud diameters varying from 80 m to less than 15 km. For the reasons already outlined the analysis is limited to measurements of the "transverse" visual diameter, of the cloud. The visual edge radius, $r_E = \frac{D_E}{2}$, is associated with a minimum integrated line-of-sight

concentration, N_s. Where the cloud image is smooth edged, densitometry indicates a Gaussian form may be a reasonable approximation beyond the optically dense cloud centers. In the irregular region, the densitometry trace reveals a bias in maximum intensity toward the solar illuminated edge of the cloud with secondary peaks in intensity toward the backside of the cloud. In Figure 5 there are typical traces about 3 and 5 minutes after release of the vapor. For later times, the predominance of these intensity peaks becomes more obvious. The distribution of intensity across the cloud has deviations from a smooth Gaussian. The bias in brightness toward the sunlit edge is related to the optical thickness of the cloud while the breakup into two or three separate intensity peaks may either be related to the effect of atmospheric turbulence or, more prosaically, the superposition of the separate streams from the three ports in the vaporizer. The existence of photographs of some earlier trails generated by a single port vaporizer will offer comparisons that might illuminate the second interpretation. For the moment, the assumption of a Gaussian distribution of vapor will also be assumed in treating the visual edge data in the irregular part of the trail. This is partially justified by restricting measurements to easily identified quasi-globular masses of vapor that characterize the irregular part of trail. The assumption of an equivalent gaussian cloud of sodium vapor relates the concentration N_s to the visible radius r_E as follows:

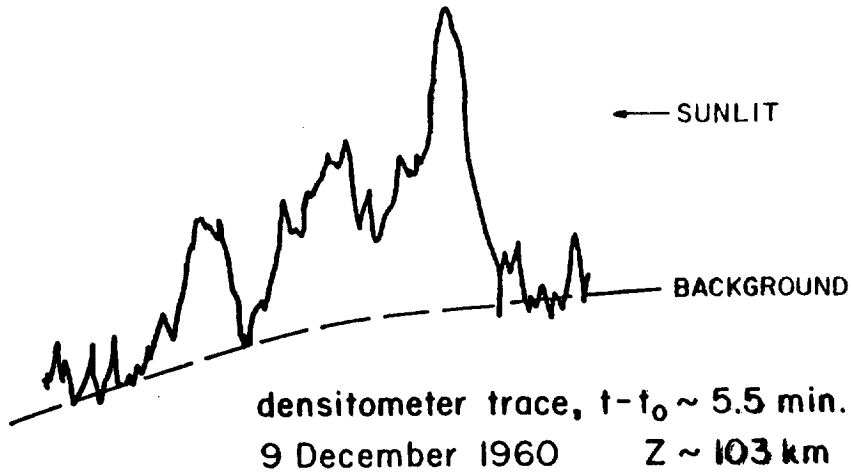

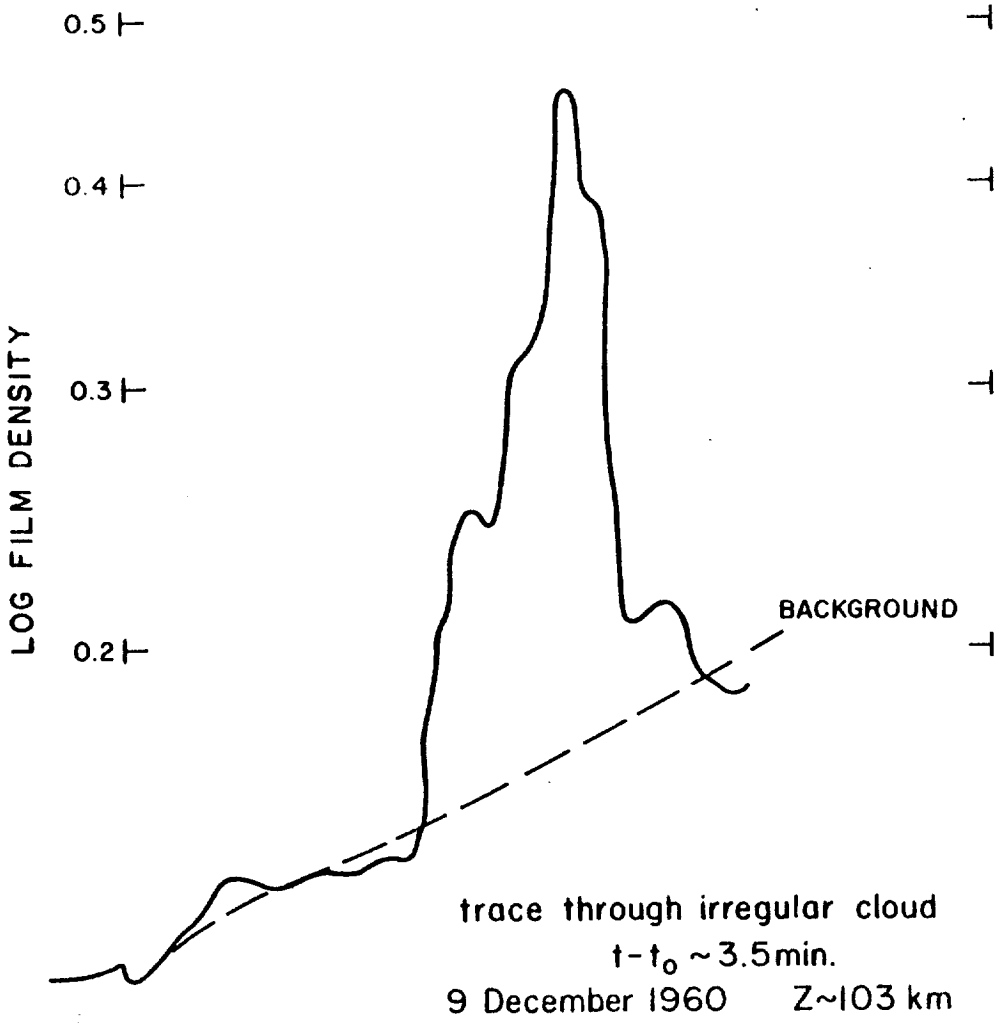

Figure 5. Typical densitometer traces across the cloud.

$$N_s = \frac{Q}{2\pi\sigma^2(t)} \exp\left[\frac{-r_E^2}{2\sigma^2(t)}\right] \qquad (4\text{-}1)$$

where r_E = radius of visible edge from cloud center

$\sigma^2(t)$ = variance of integrated line-of-sight distribution

Q = total number of sodium atoms per unit length of cloud

N_s = minimum integrated line-of-sight concentration of sodium atoms emitting resonant radiation which will make a visual contrast with the sky background darkening.

If the sky background were constant, the "concentration" N_s would be constant and a relation between $\sigma^2(t)$ and r_E^2 is obtained from the Relation (4-1) and $\frac{dN_s}{dt} = 0$, so that

$$\frac{d(r_E^2)}{dt} = \frac{d(\sigma^2)}{dt}\left(\frac{r_E^2 - 2\sigma^2}{\sigma^2}\right) \qquad (4\text{-}2)$$

The maximum visible radius of the cloud, $\rho^2 = r_{E_{max}}^2$, is defined by $\frac{dr_E}{dt} = 0$. At this instant the variance is related to the visible edge by $\sigma^2 = \frac{1}{2} r_E^2$ and

$$\frac{N_2}{Q} = (2\pi\rho^2/2)^{-1} \exp(-1) = (2\pi\sigma^2)^{-1} \exp\left[-\frac{r_E^2}{2\sigma^2}\right] = \text{constant} \qquad (4\text{-}3)$$

By taking the logarithm of this relation, the variance at any instant is shown to be related to visible edge radius by

$$\sigma^2(t) = \frac{r_E^2}{2}\left[\ell n\left(\frac{\rho_e^2}{2}\right) - \ell n\sigma^2(t)\right]^{-1} \qquad (4\text{-}4)$$

This is the equation used by Kellogg[11] and Gifford[12] in their analysis of smoke puff data in the stratosphere.

In the sodium twilight experiments, the background is not constant over the period of the photographic sequence. This period, which varies between 10 and 12 minutes typically, corresponds to solar depression angles of 6 to 9 degrees.

The ratio, N_s/Q,

$$\frac{N_s}{Q} = (2\pi\sigma^2)^{-1} \exp\left[-\frac{r_E^2}{2\sigma^2}\right] \qquad (4\text{-}5)$$

is not constant within the observation time of the clouds. During the evening twilight $\frac{dN_s}{dt}$ is expected to approach zero through negative values; in the morning twilight, it is expected to be zero during pre-observation times and then become positive at some unknown rate. The modifications that these facts introduce into Equations (4-3) and (4-4) are as follows: If we designate three times: t_1, t_2, and t_3 such that

$$t_1: \frac{dN_s}{dt} = 0$$

$$t_2: \frac{dr_E}{dt} = 0$$

$$t_3: r_E^2 = 2\sigma^2$$

then the following sequence of events is possible:

morning twilight

$$t_1 < t_2 < t_3; \frac{dN_s}{dt} > 0 \text{ for } t > t_1$$

evening twilight

(a) $t_1 < t_2 = t_3 \quad \frac{dN_s}{dt} < 0 \text{ for } t < t_1$

(b) $t_3 < t_2 < t_1 \quad \frac{dN_s}{dt} < 0 \text{ for } t < t_1$

In case (a) for an evening twilight, the method may be used directly; some overestimation of σ^2 values occurs for diffusion times less than t_1. For the other cases, the changing background introduces the following modifications for a quasi-spherical cloud:

$$2\pi \frac{N_s}{Q}(t) \neq 2\pi \frac{N_s}{Q}(t + \Delta t)$$

but

$$2\pi \frac{N_s}{Q} = \frac{1}{\sigma^2} \exp\left[-\frac{r_E^2}{2\sigma^2}\right] = \left(\frac{\rho^2 e}{2}\right)^{-1} + \delta \qquad (4\text{-}6)$$

where

$$\delta \sim \frac{2\pi}{Q} \frac{dN_s}{dt} \Delta t$$

Taking the time derivative of (4-1) now gives

$$\frac{2\sigma^2}{N_s} \frac{dN_s}{dt} + \frac{dr_E^2}{dt} = \frac{d\sigma^2}{dt}\left(\frac{r_E^2 - 2\sigma^2}{\sigma^2}\right) \qquad (4\text{-}7)$$

taking the logarithm of (4-6) reduces to

$$\sigma^2 = \frac{r_E^2}{2}\left[\ell n(\rho^2 e) - \ell n(2 + \rho^2 e\delta) - \ell n\sigma^2\right]^{-1} \qquad (4\text{-}8)$$

The corresponding equations for a quasi-cylindrical cloud are:

$$\sqrt{2\pi} \frac{N_s}{Q} = (\sigma^2)^{-\frac{1}{2}} \exp\left[-\frac{r_E^2}{2\sigma^2}\right] = (\rho^2 e)^{-\frac{1}{2}} + \delta \qquad (4\text{-}6a)$$

$$\frac{2\sigma^2}{N_s} \frac{dN_s}{dt} + \frac{dr_E^2}{dt} = \frac{d\sigma^2}{dt}\left(\frac{r_E^2 - \sigma^2}{\sigma^2}\right) \qquad (4\text{-}7a)$$

$$\sigma^2 = r_E^2\left[\ell n(\rho^2 e) - \ell n\sigma^2 - 2\ell n\left(1 + \delta(\rho^2 e)^{\frac{1}{2}}\right)\right]^{-1} \qquad (4\text{-}8a)$$

The application of either formula depends upon the appearance of the cloud at the height where measurements of the lateral diameter are to be made. For a cloud of globular irregularities the spherical cloud is assumed; for a smooth cylinder whose axis is perpendicular $\pm 30^{o}$ with the optical axis of the camera, a cylindrical cloud is assumed. For an actual sequence of r_E^2 values the resulting σ^2, using either set of equations, will have the same time dependency, say $\sigma^2 = Kt^2$. The difference is the larger K value for the assumption of a cylindrical cloud then for a spherical one. (See Figure 8).

In preliminary measurements of the transverse growth of the cloud, the photographs of the following trails are used:

24 May 1960	(PM)
9 December 1960	(AM)
20 April 1961	(PM)
17 September 1961	(AM)

The Wallops Island 7" negatives were used in all cases except 24 May 1960 where the 70 mm data were used. In addition, measurements were made from the 17 September 70 mm data.

Figure 4 is a composite of four photographs taken at Wallops minutes after the rocket was fired on 9 December 1960 (AM) and 17 September 1961 (AM). On 9 December the transition after the long straight stretch of irregular cloud is at 104.5 km and the corresponding

break after the straight stretch in the downtrail also occurs at 104.5±2. The bottom end of the straight irregular stretch is at 97 km. Measurements of the radial growth were made in two regions: 98-102 km (irregular trail) and 113-117 km (smooth). This last region corresponds to the smooth trail which intersects the irregular trail and is also superposed against a higher part of the smooth upper trail. Because of this superposition the unlit backside of the trail is outlined against the illuminated trail directly above. Thus a good estimate of the width of the sodium vapor is obtained.

In Figure 6, the data for the upper layer are seen to be consistent with a purely molecular dispersion process. The growth of the visual trail in the lower region is accelerated and some other mechanism besides molecular diffusion is implied. The photographic sequence was terminated before the $r_{E\ max}$ could be determined. The σ^2 values for curve (b) were computed for an $r_{E\ max}$ estimated by the fall off in the r_E^2 values from the curve. The unexpected deviation from the $\sigma^2 \sim t$ curve after 300 seconds would imply a deviation from a purely molecular dispersion if the exact value of ρ^2 had been determined empirically. However, an underestimation of ρ^2 and the increasing background effect δ must be considered in interpreting this result. In morning twilight the value of δ is expected to be positive. However, to reduce σ^2 - values to the spiked circle value on the graph for any ρ^2 greater than the original estimate of $\rho^2 \approx 3.48\ km^2$ and up to $\rho^2 = 4.6815$, the

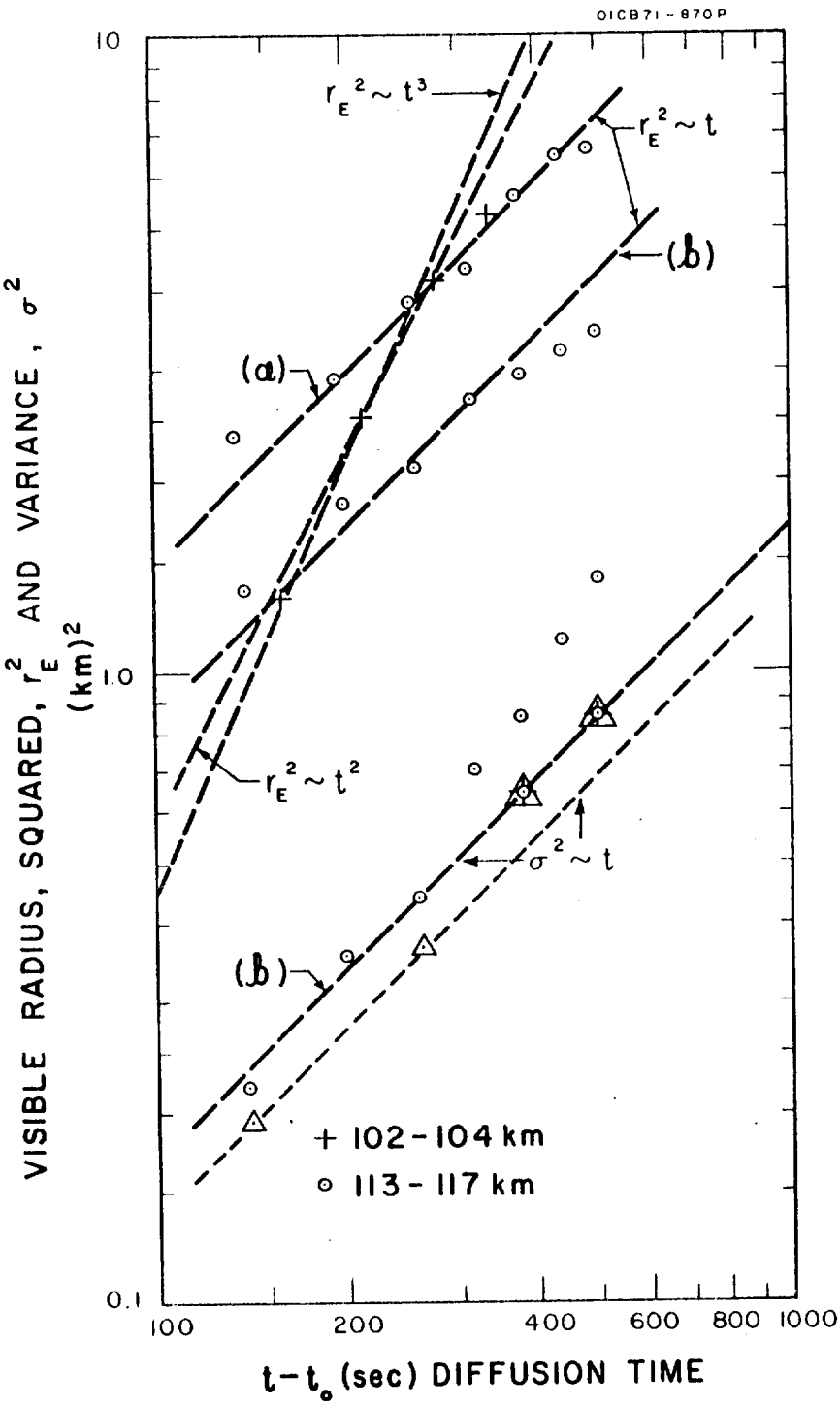

CLOUD EXPANSION DATA
9 DECEMBER 1960

Figure 6.

required values of δ are negative. This contradicts our physical intuition about the sign of δ which, it is argued, should be positive in a morning twilight release. If the actual r_E^2 curve b is extrapolated, a value of $\rho^2 \simeq 4.682$ would occur at $t - t_o \simeq 900$ seconds. This is not an unreasonable result for this altitude when comparison is made with the 17 September 1961 case where the maximum visual diameter occurred at $t - t_o = 820$ seconds. The corresponding σ^2 values for $\rho^2 \simeq 4.682$, $\delta = 0$ are indicated by the $\triangle$ in Figure 6. The resulting curve through the $\triangle$ points greater than 300 seconds is superposable on the $\sigma^2 \sim t$ curve for $\triangle$ points less than 300 seconds with an $\delta/2\pi$ value of 6×10^{-3}. The value of the molecular diffusion coefficient deduced from the latter curve is

$$D \sim 6.8 \times 10^6 \text{ cm}^2/\text{sec}$$

--A very reasonable value when compared with other determinations[4] in the 113-114 km region.

A striking feature of the distribution of $\triangle$ points is the apparent parallel displacement of the two segments either side of $t - t_o \sim 300$ seconds. This is more suggestive of a discrete change associated with adjusting lens openings rather than the continuously changing background intensity.

In the above analysis of the radial expansion in the region where only molecular dispersion is expected, the importance of empirical determination of $r_{E\,max}^2$ and consideration of background and lens aperature changes is indicated. In the measurement of r_E^2 values for two evening shoots of which Figure 7 is the r_E^2 data for 24 May 1960, the sequence of photographs terminated before $r_{E\,max}^2$ could be determined and no σ^2 values were computed. In the other morning twilight, 17 September 1961, measurements were made on both Wallops Island negatives, which terminated before a definite $r_{E\,max}^2$ could be determined, and on 70 mm negatives from a site 159.7 km to the northwest of Wallops Island. These latter sequences of negatives were of sufficient length to allow the $r_{E\,max}^2$ to be determined: $r_{E\,max}^2 = 14\ km^2$ at $t - t_o = 820$ seconds. Figure 8 represents the r_E^2 data and σ^2 values for both quasi-spherical and quasi-cylindrical clouds. Both cloud-form assumptions yield $\sigma^2 \sim t^2$ up to $t - t_o \sim 695$ sec at which time there is a transition to $\sigma^2 \sim t^\alpha$ where $\alpha \sim 4.4$. This α value would be modified if background changes were included in the computation of σ^2.

In either Equation(4-7) or(4-7a), a positive value of $\frac{2\sigma^2}{N_s}\frac{dN_s}{dt}$ requires a corresponding negative value for $\frac{dr_E^2}{dt}$. The time when $r_E^2 = 2\sigma^2$ (Equation 4-7) or $r_E^2 = \sigma^2$ (Equation 4-7a) is some time after the time when $\frac{dr_E}{dt} = 0$. Thus, the proper value of r_E^2, where $r_E^2 = \sigma^2$, is less than $r_{E\,max}^2$ and the α value, $\alpha \sim 4.4$, is larger than it would be if the proper r_E^2, $r_E^2 < r_{E\,max}^2$, had been used to compute the σ^2 values in Figure 8.

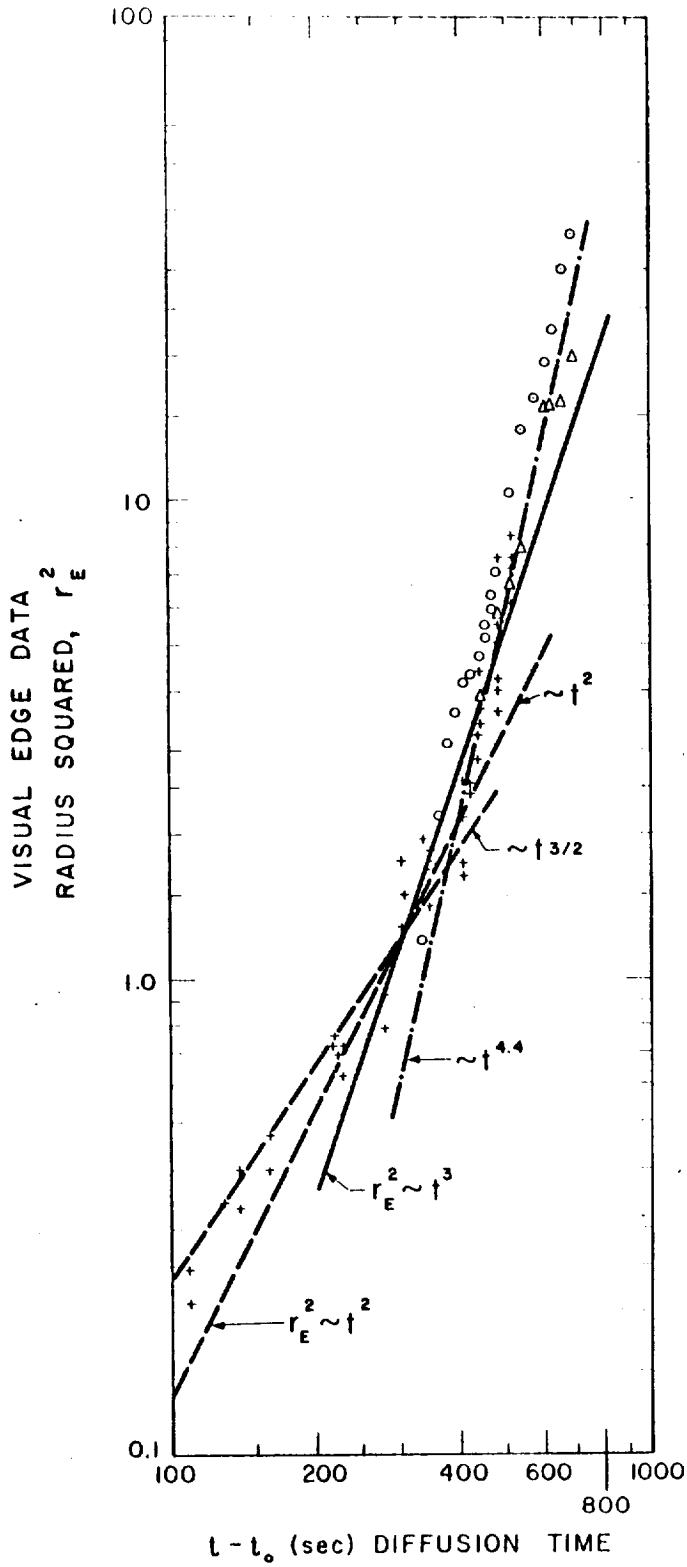

CLOUD EXPANSION DATA
24 MAY 1960 (PM)
108 – 110 km

Figure 7. Cloud expansion data, 24 May 1959 (PM).

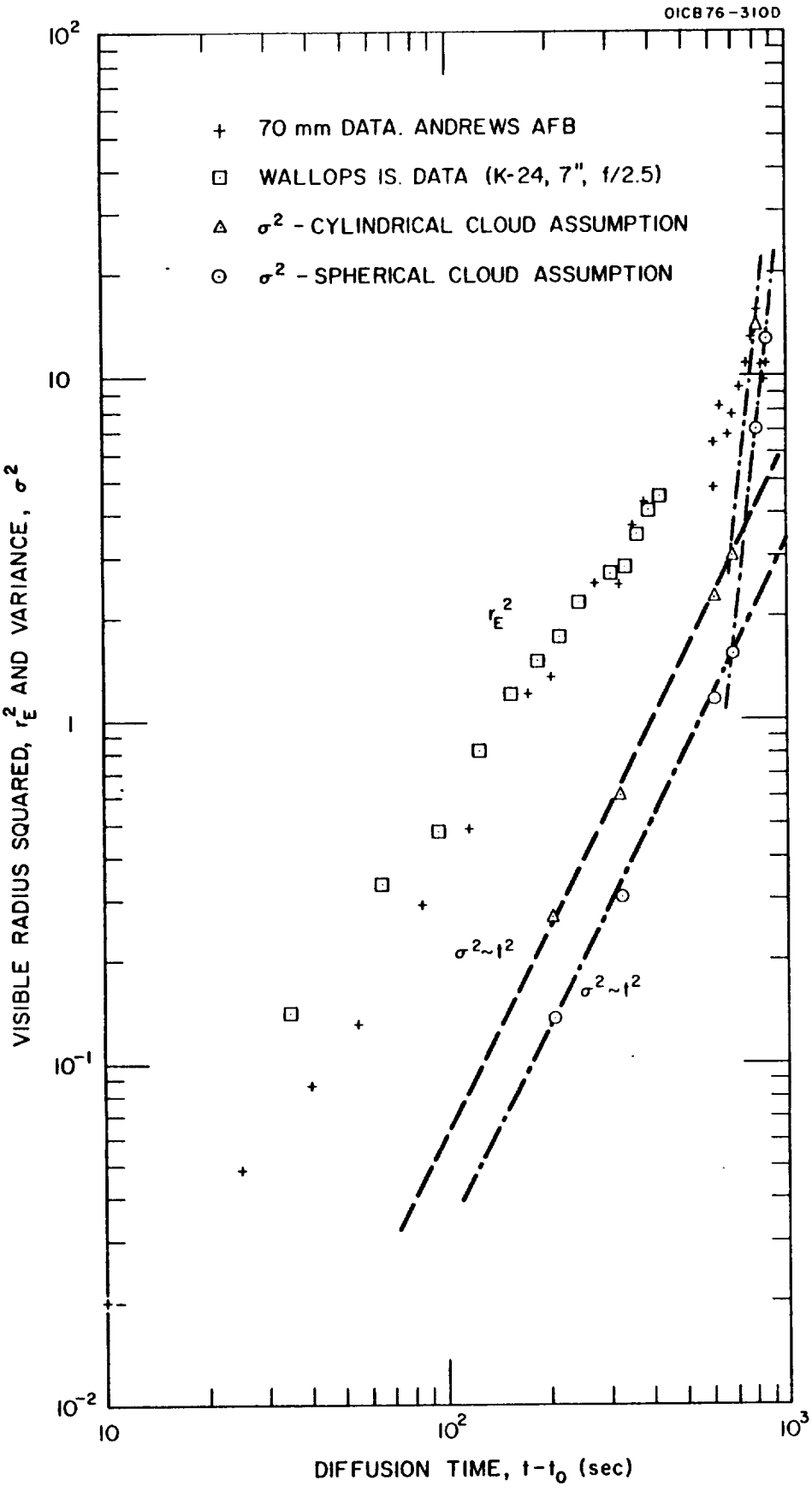

Figure 8. Cloud expansion data, 17 September 1961 (AM).

Analysis of the 9 December 1960 and 17 September 1961 data indicate some of the difficulties in extracting meaningful indications of dispersion in the upper atmosphere. Above 111 km the transverse expansion of the cloud indicates a compatibility with a purely molecular diffusion. Below 111 km in the 100 to 108 km region, the radial expansion of the cloud proceeds more rapidly than can be explained by molecular diffusion alone. Before invoking pre-existing atmospheric turbulence as the necessary mechanism for the accelerated dispersion, the rocket associated disturbances, wake and jet release of vapor, should be eliminated.

SECTION 5

WAKE REYNOLDS NUMBER

Townsend[14] has reviewed the experimental evidence of wake behavior as a function of wake Reynolds number, $\frac{U_1 d}{\nu}$. The following is briefly what is expected: For wake Reynolds numbers,[15] less than 40 the wake flow is steady and laminar. Above 40 and less than $R_d = 60$, the laminar wake is unstable to small disturbances. Probably up to $R_d = 120$, the wake would consist of the familiar vortex street formed by the periodic shedding of vortices. At $R_d \geq 5 \times 10^5$ the boundary layer on the surface becomes turbulent and evidence will be present to show that these high Reynolds numbers are not attained by these rockets.

The diameter of the nose cone is about 6 inches (.15 meters). The effective diameter that the travelling rocket presents to the atmosphere is larger than this and we consider d = 1 meter to be a reasonable upper bound. The velocity of the rocket is available from the radar trajectory data. Table 1 is a summary of results.

TABLE 1

WAKE REYNOLDS NUMBERS AT CERTAIN HEIGHTS FOR TYPICAL ROCKET AND ATMOSPHERIC PARAMETERS

Z (km)	U (m/sec)	ν (m^2/sec)	R_d
58	1570	$\approx 4 \times 10^{-2}$	6×10^4
95	1200	$\approx 4/5$	300/250
104	1150	≈ 30	40

In this type of argument, the variability from U_∞, the rocket velocity and d, the effective rocket diameter, are much less than ν, where $\nu = \nu\ (P,T)$.

SECTION 6

TURBULENT WAKE AND JET

Power laws for behavior of width and maximum center-line velocity in turbulent wakes and jets are given in the textbook by Schlichting,[16]

	Laminar		Turbulent	
	Width	Center-Line Velocity	Width	Center-Line Velocity
Circular Jet	x	x^{-1}	x	x^{-1}
Circular Wake	$x^{\frac{1}{2}}$	x^{-1}	$x^{1/3}$	$x^{-2/3}$

where x is the distance behind the object producing the wake or the distance in the jet from the nozzle. A recent laboratory study of the turbulent trail behind a hypervelocity sphere has reproduced a wake growth power law $x^{1/3}$ for 1 atmosphere pressure, 11 mm Hg, and 41 mm Hg (Slattery and Clay[17]). The application of these laws to the sodium releasing rocket gives the following predictions

TABLE 2

COMPARISON OF PREDICTED WAKE DIAMETERS WITH ACTUAL CLOUD DIAMETERS

$t = \frac{x}{1000 \text{ m/sec}}$	x	Predicted Wake Width (Meters)		Measured Dia. of Sodium Cloud	Ratio
		Turbulent	Laminar		
10 sec	10^4 meters	43	100	270 m	
30 sec	3×10^4	62	173	312 m	.2
100 sec	10^5	94	316	1100 m	.08
300 sec	3×10^5	134	548	2100 m	.06

After 10 seconds the maximum velocity of the wake would be diminished by $\frac{1}{400}$. An upper bound may be given for the maximum turbulent velocity in the wake after 10 seconds by

$$\frac{1000}{400} = 2.5 \text{ m/sec}$$

and after 30 seconds

$$\frac{1000}{3600} = 0.3 \text{ m/sec}$$

which is 1/10 of the root mean-square velocity computed from the growth of the trail during the diffusion time interval 35 - 365 seconds. From these rough considerations, we should expect the effect of a turbulence induced by the passage of the rocket to be negligible after 35 seconds. This expection would not be valid if these rocket associated disturbances interacted with the atmospheric strain field, indicated by the large variation of horizontal velocity over depths of 7 to 10 km. Smaller scale internal gravity waves might also be expected to exist in this stably stratified region of the upper atmosphere. The predictions given above are valid in wind tunnels (and other experimental situations) where the turbulence once generated decays with time. To point to this interaction as a means of maintaining the rocket generated turbulence, one must also be prepared to justify their preferment over other possible disturbances and why these are not amplified in time also.

SECTION 7

RICHARDSON NUMBER AND THE STABILITY OF THE UPPER ATMOSPHERE

Although the answer to this question is not available, it is of interest to draw certain inferences from the wind profile data. The maintenance of turbulent motion is related to the non-dimensional ratio R_f, the flux Richardson number[18]

$$R_f = \frac{g_i}{T} \overline{\theta u_i} \Big/ \left[\overline{u_j \cdot u_e} \frac{\partial U_j}{\partial x_e} \right]$$

If the Reynolds stress, $\overline{u_j u_e}$, and temperature-velocity fluctuation correlation $\overline{\theta u_i}$ are representable by mean gradients, then

$$R_f = f(R_i)$$

where

$$R_i = \frac{g}{\hat{\rho}} \frac{d\hat{\rho}}{dz} \Big/ \left(\frac{\partial u}{\partial z} \right)^2 + \left(\frac{\partial v}{\partial z} \right)^2 = \frac{N^2}{\left(\frac{\partial u}{\partial z} \right)^2 + \left(\frac{\partial v}{\partial z} \right)^2}$$

$\hat{\rho}$ = potential density

N = Brunt-Väisälä frequency

Some indications of the magnitude of R_i are available from a single sounding over Fort Churchill, Canada, in 1958. The magnitude of R_i in the 100 to 108 km region is greater than one and less than 3.4. The variability is due to the variability in the virtical shear rather than the Brunt-Väisälä frequency. (Table 3).

TABLE 3

FORT CHURCHILL, CANADA				OCTOBER 31, 1958		
Z km.	density-ρ $gr/m^3 x10^{-4}$	pressure-p mm Hg x 10^{-4}	T(^oK)	Z	$\frac{1}{\hat{\rho}} \frac{d\hat{\rho}}{dz}(m^{-1}x10^{-4})$	$N^2(sec^{-2}x10^{-4})$
98	9.48	4.52	221.5			
				99	1.22	11.6
100	6.86	3.37	227			
				1Q2	1.14	10.8
105	3.20	1.68	245			
				105	1.20	11.39
110	1.54	0.87	262			
				107.5	1.10	10.4
Viking 7 data - White Sands, New Mexico						
100	2.50	1.10	210			
				105	1.20	11.34
110	0.50	0.26	228			
				115	1.10	10.34
120	0.12	0.08	270			

Brunt-Väisälä frequency, N from the Viking-7 data, White Sands, New Mexico[19] and pitot-static measurements, Fort Churchill, Canada.[20]

An average stability of the 98 to 115 km region as indicated by this data is $N^2 \sim 11 \times 10^{-4}$ sec^{-2}. The average value that has been assumed in other studies is $N^2 \sim 4 \times 10^{-4}$ sec^{-2}. If such a stable atmosphere is assumed to be valid over Wallops Island, Virginia, then the vertical shear has a minimum magnitude necessary to satisfy a theoretical Richardson number criteria for turbulence.

	$N^2 = 11 \times 10^{-4}$ sec^{-2}	$N^2 = 4 \times 10^{-4}$ sec^{-2}
for Ri < 1	$\frac{\partial u}{\partial z} > 33 \sin \phi$ m sec^{-1} km^{-1}	$\frac{\partial u}{\partial z} > 21 \sin \phi$ m sec^{-1} km^{-1}
	$\frac{\partial v}{\partial z} > 33 \cos \phi$ m sec^{-1} km^{-1}	$\frac{\partial v}{\partial z} > 21 \cos \phi$ m sec^{-1} km^{-1}
for Ri < $\frac{1}{4}$	$\frac{\partial u}{\partial z} > 66.5 \sin \phi$ m sec^{-1} km^{-1}	$\frac{\partial u}{\partial z} > 40 \sin \phi$ m sec^{-1} km^{-1}
	$\frac{\partial u}{\partial z} > 66.5 \cos \phi$ m sec^{-1} km^{-1}	$\frac{\partial u}{\partial z} > 40 \cos \phi$ m sec^{-1} km^{-1}

The direct application of the above criteria for shear would suggest that turbulence would be confined to narrow layers in the upper atmosphere. Figures 9 and 11 illustrate vertical wind profiles for two of the clouds used in this study. Figure 10 gives the distribution of vertical shear. It should be remarked that in both cases diameter

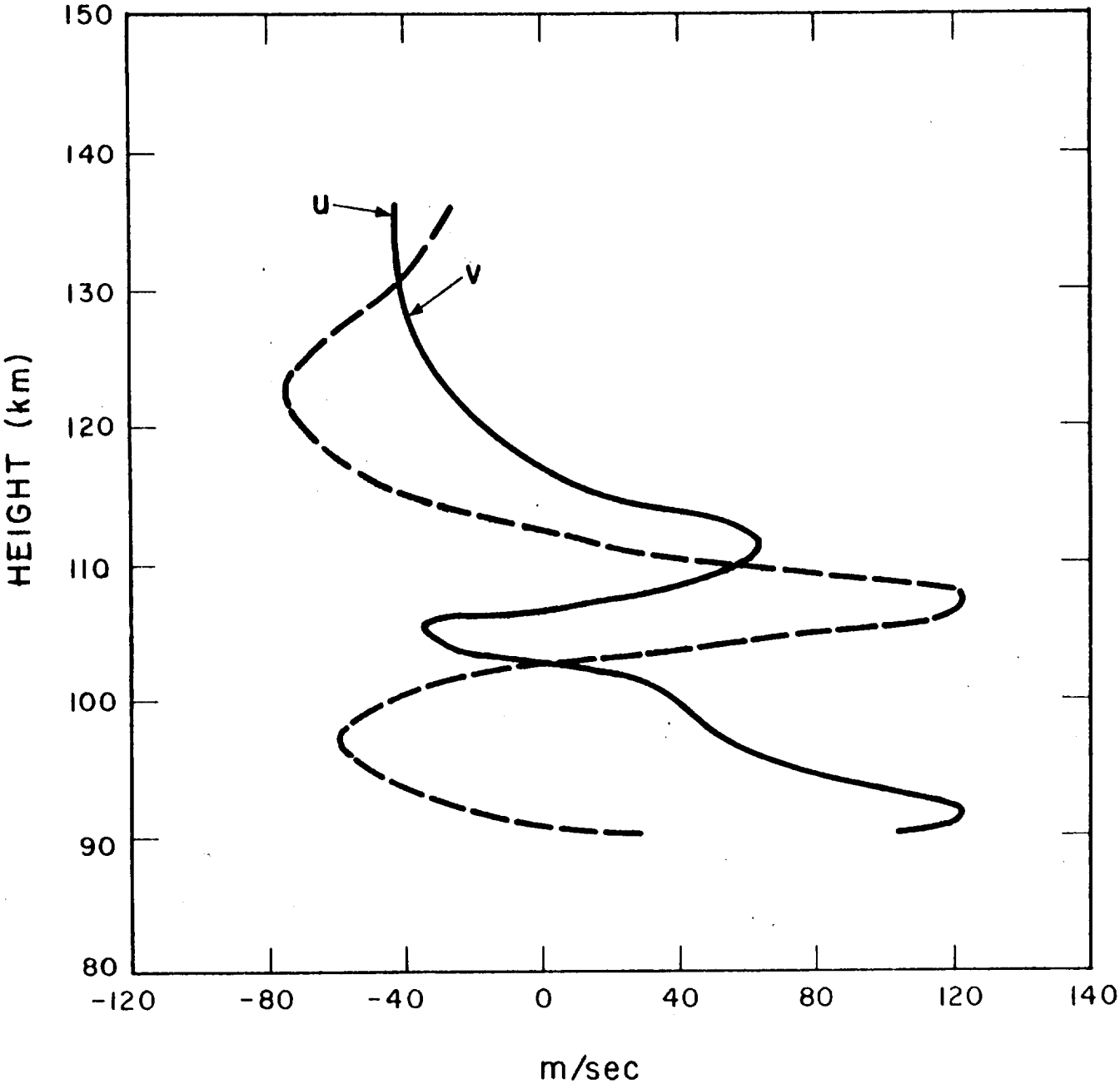

WIND VELOCITY COMPONENTS
9 DECEMBER 1960 (AM)

Figure 9.

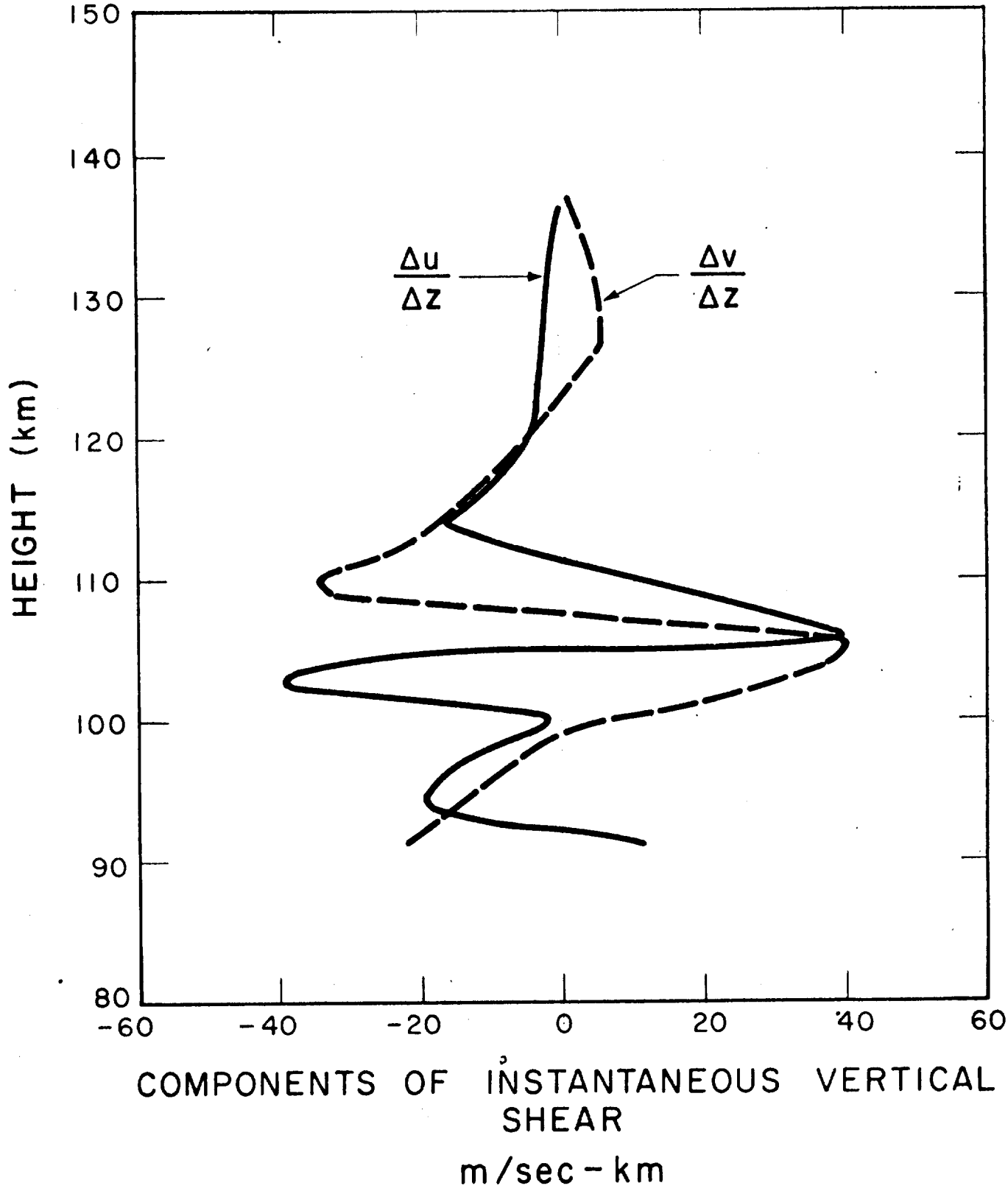

SHEAR COMPONENTS
9 DECEMBER 1960 (AM)

Figure 10.

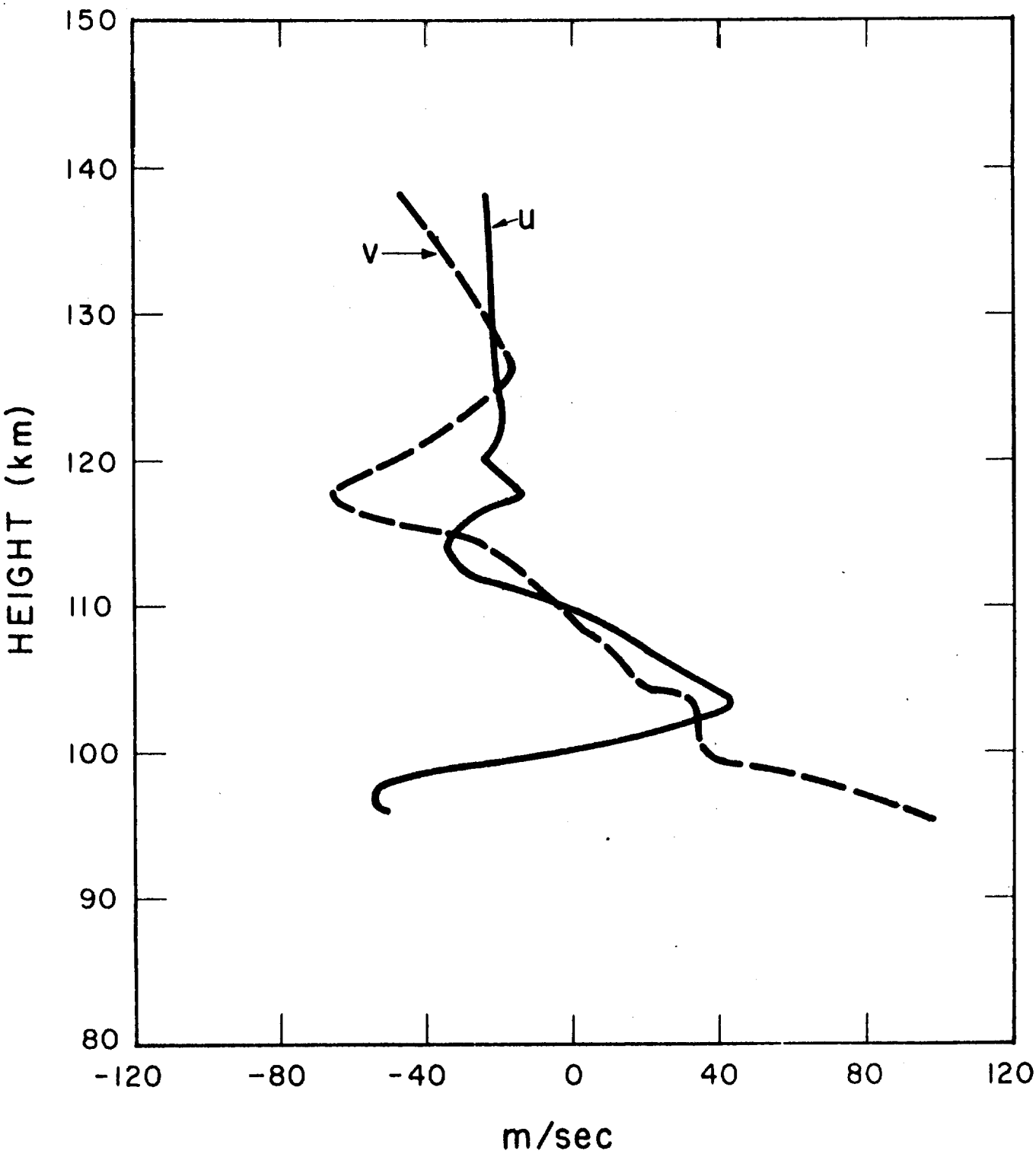

WIND VELOCITY COMPONENTS 17 SEPTEMBER 1961 (AM)

Figure 11.

measurements in the irregular part of the clouds were made in regions of high shear. Although Figure 10 indicates no region where the more stringent requirement on the shear, $\frac{\partial u}{\partial z} > 65 \text{ sec}^{-1}$ is satisfied, there is enough uncertainty in the theoretical determinations of the relationship, $R_f = f(R_I)$ to make exclusion of turbulence when $R_i > 1/4$ equally uncertain.

SECTION 8

COMPARISON WITH PREVIOUS STUDIES

Meteor trails and rocket generated sodium trails have been analyzed by Greenhow[21] and Blamont et alia.,[5,22] respectively, for evidence of turbulence in the upper atmosphere. In both studies, the radial expansion of the luminous intensity, which is 1/e of the intensity of the cloud center, is taken as a measure of the cloud dispersion. Greenhow's data refer to the 90 km height; Blamont's data refer to some height below 102 km. Figure 12 is a reproduction of Greenhow's four points, Blamont's two points, and the σ^2 curves from Figure 11. Both investigations have assumed the validity of an $r^2 \sim \epsilon t^3$ law. Since there are so few points, it is difficult to utilize their results to convince the skeptic about the applicability of the inertial subrange predictions of similarity theory at these heights. Greenhow's two points beyond $t - t_o = 300$ sec are parallel to the $t^{3/2}$ line.* Prior to 300 seconds, the curve connecting the other two points falls between the $r \sim t^{1/2}$ and $r \sim t$ curves. Assuming that the similarity theory is applicable, meteor trail data could be fitted to the similarity

*Greenhow's ordinate is standard deviation not variance

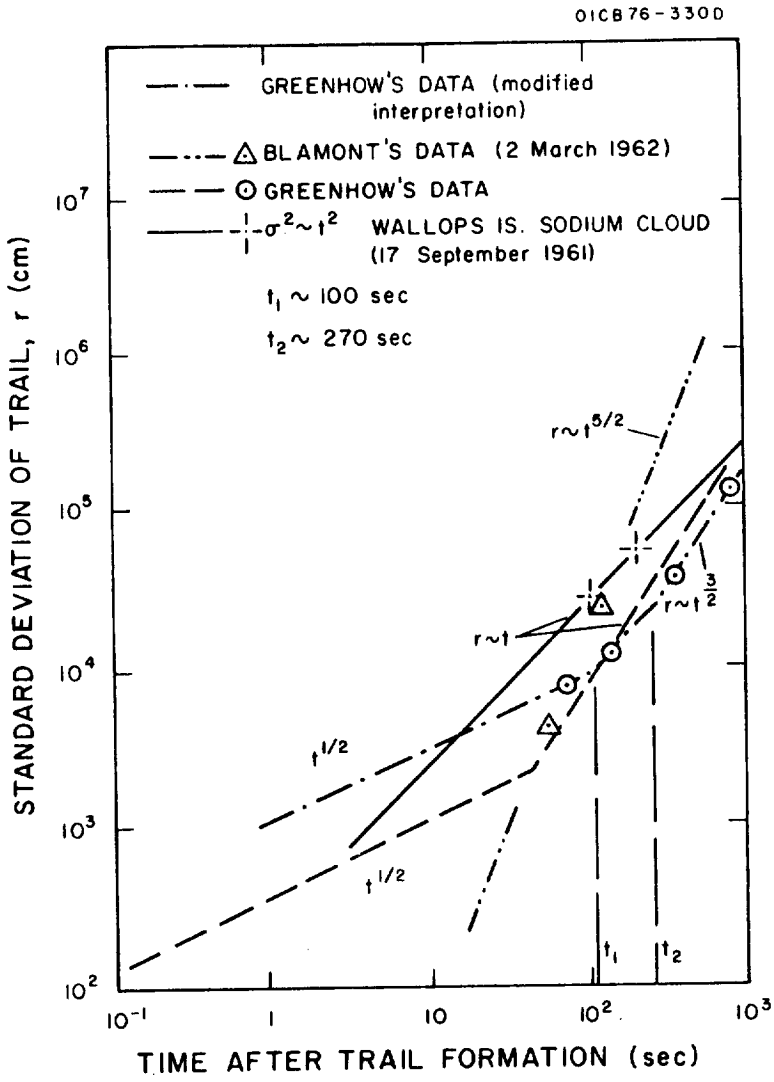

Figure 12. Comparison of meteor and sodium trail data.

predictions by fitting a $t^{1/2}$ curve through the first point a t curve through the second and a $t^{3/2}$ curve through the last two. Two transition times, t_1 and t_2 are defined by the three curves; $t_1 \sim 100$ seconds and $t_2 \sim 270$ seconds. Because we have displaced Greenhow's original curve $r \sim t^{3/2}$, the estimate of ϵ, the turbulent dissipation by extrapolating the $t^{3/2}$ back to t = 1, is reduced to $\epsilon \sim 20$ ergs g^{-1} sec^{-1}. From the t_2 value, we may determine another estimate of ϵ using the relationship of Gifford[12] and Batchelor,[10] $t_2 \sim y_o^{2/3}\ \epsilon^{-1/3}$. This estimate is $\epsilon \sim 10^{-2}$ ergs g^{-1} sec^{-1} ($\epsilon \sim 5 \times 10^{-2}$ when $y_o \sim 10^3$ cm). The small segment of $r \sim t$ curve may be extrapolated back to t = 1 where $r = 10^2$ cm

(a) $\langle r^2 \rangle \sim \epsilon t^3$ at $t = 1 \Rightarrow \epsilon \sim 20$ ergs g^{-1} sec^{-1}

(b) $\langle r^2 \rangle \sim (\epsilon r_o)^{2/3} t^2$ at $t = 1$, $r_o = 10^3$cm $\Rightarrow$ $\epsilon \sim 10^3$ ergs g^{-1} sec^{-1}

(c) $\epsilon t^3 \sim (\epsilon r_o)^{2/3} t^2$ at $t = t_2$, $r_o = 10^3$cm $\Rightarrow \epsilon \sim 10^{-2}$ergs g^{-1} sec^{-1}

The discrepancy between these results is obvious. While neither (a) nor (b) have been used to assess ϵ in the lower atmosphere, (c) has and is reported to give results[13] comparable with the methods of direct sampling of velocity fluctuations. Thus, if one were to accept a determination of an $\langle r^2 \rangle \sim t^3$ growth law by only two points, the applicability of inertial subrange dispersion predictions, and the existence of small scale isotropic turbulent velocity components, then

following the Batchelor[10] - Gifford[12] reasoning, the turbulent dissipation, ϵ, indicated by the meteor data is closer to a value of 5×10^{-2} ergs g^{-1} sec^{-1} than 70 ergs g^{-1} sec^{-1} reported by Greenhow and Blamont. Blamont's two points, although comparable in magnitude with both the meteor and Wallops data, indicate an expansion law $\langle r^2 \rangle \sim t^5$ if connected directly. The Blamont data at 120 seconds compares closely with the σ^2 value at the same time. The value at 60 seconds is much smaller than comparable σ^2 for the Wallops data at 60 seconds. If more points beyond 120 seconds had been measured by Blamont, then this exceptional growth would have either been confirmed or not. Without this confirmation, its validity is speculative.

Qualitatively, there is one significant difference between the French Sahara sodium trails and those at Wallops Island. The lower, irregular appearance of the cloud is reported to become smooth in both up-trail and down-trail at the same height. This is not true of the Wallops Island trails (see Figure 4), where the down-trail transition is consistently lower in height than the up-trail. This fact,coupled with the persistence of their shape from seconds after release of the rocket to four or five minutes time,strongly suggests their origin in formation mechanisms of the cloud, rather than the effect of pre-existing atmospheric turbulence.

Other explanations for the transition are related to the ratio of density in the jet to atmospheric density and to the increasing ability of molecular diffusion to smooth in the irregularities associated with the initial deposition of the vapor. With an average sodium charge of 2 kg, up to 5 x 10^{25} atoms are available for deposition into the atmosphere. If 80% of these atoms are produced by the vaporization, deposited into a trail 100 km long by 7 to 8 meters in diameter, the average spatial density is $\sim 10^{13}$ atoms/cm^3. The atmospheric density is $\sim 10^{13}$ atoms/cm^3 at 108 km, (104-112 in the standard atmosphere). The value of 108 km is only an approximate estimate but somewhere in the 90 to 112 km region, the density of sodium vapor jet becomes equivalent to and then greater than the ambient density. It is also near 110 km that the measured diffusion coefficients of $D \sim 10^7$ cm^2 sec becomes large enough to explain the transition in appearance of the cloud. If the irregularities are due to a turbulent jet, then the size of the disturbance is limited by the overpressure within the cylinder and the diameter of the exhaust port. Particularly during uptrail these are constant. The possibility now exists that irregularities within the turbulent jet are smoothed by the rapid expansion of the vapor in the ambient atmosphere. This problem of the transition is interesting but secondary to the question of the existence of turbulence which will be confirmed or disproved by the dispersion of the cloud.

SECTION 9

CONCLUSIONS

The radial expansion of the cloud indicates molecular diffusion is the dominant dispersion mechanism above 110 km. Below this height both the meteor trail data and the sodium trail data indicate a growth rate greater than that associated with molecular diffusion. In the 100 to 108 km height region, the association of this accelerated growth with pre-existing atmospheric turbulence is not conclusively established. Although the meteor trail data indicates a $\langle r^2 \rangle \sim t^3$ growth at 90 km between 270 and 900 seconds after the passage of the meteor, the confirmation of a similar transition in the growth of the sodium trails at heights of 100 to 108 km must await the assessment of the corrections for background and lens opening changes on the functional form of σ^2. On 9 December, an assurance that molecular dispersion is the predominant mechanism, in trail growth at 112 km, allowed determination of a δ value necessary to reduce the computed σ^2 values for late diffusion times to a $\sigma^2 \sim t$ curve for early diffusion times. By this means an empirical determination of $\delta \sim \frac{1}{Q} \frac{dN_s}{dt}$ is possible. By choosing those trails where there is overlapping of the trail images (see Figure 4) on the

Wallops Island negatives, these δ values would be valid for the higher regions where molecular diffusion predominates and also those lower heights where we are specifically interested in the possible existence of turbulence.

The transition in the σ^2 curve, whose existence is very sensitive to the empirical evaluation of r_E, δ, and the r_E value when $\frac{2\sigma^2}{N_s}\frac{dN_s}{dt} + \frac{dr_E^2}{dt} = 0$, can then be evaluated. The existence of $\sigma^2 \sim t^{\alpha}$ where $\alpha = 3$ would correspond with the similarity theory predictions.[16] Any other value of α greater than 2 would offer stimulation to some of the more recent theoretical studies by Bolgiano and Roberts.

APPENDIX

I. STATIONARY ANISOTROPIC DISPERSION BY CONTINUOUS MOVEMENTS

In an analysis which appears to relax some of the restrictions necessary in the dimensional arguments based upon Kolmogorov's theory i.e. a large Reynolds number of turbulence, C. C. Lin has predicted a time dependence of t^3 for the relative dispersion $\langle Y_i Y_j \rangle$. Lin's theory of dispersion assumes that the forces acting on the dispersing particles may be described by a stationary random anisotropic process but the relative velocity covariance may not:[23]

$Y_i(t)$ = component of relative displacement

$\dot{Y}_i(t) = v_i(t)$ = component of relative velocity

$\dot{v}_i(t) = a_i(t)$ = component of relative acceleration

$$\langle a_i(t')a_j(t'') \rangle = \alpha_{ij}(\tau) \qquad \tau = t' - t''$$

but $$\langle v_i(t')v_j(t'') \rangle \neq S_i(\tau)$$

The final form of the theory is an asymptotic result for diffusion times within a certain time interval $\tau_1 < t < \tau_2$ to be defined by the time τ_1, where the covariance sum $A_{ij} = \frac{1}{2}(\alpha_{ij}(\tau) + \alpha_{ji}(\tau)$ is negligibly small. The time $\tau_2 > \tau_1$ although greater than τ_1, is still small enough so that the relative velocity autocorrelation is not independent of diffusion time.

Given that

$$Y_i(o) = 0, \; v_i(o) = 0$$

then $$Y_i(t) = \int_o^t (t-t')a_i(t')dt'$$

and $$\langle Y_i(t)a_j(t)\rangle + \langle Y_j(t)a_i(t)\rangle = 2\int_o^t \tau \left(\alpha_{ij}(\tau) + \alpha_{ji}(\tau)\right) d\tau$$

$$= 2\int_o^t \tau\, A_{ij}(\tau)d\tau$$

or $$\frac{d^2}{dt^2}\langle Y_i(t)Y_j(t)\rangle - 2\langle v_i(t)v_j(t)\rangle = 2\int_o^t \tau\, A_{ij}(\tau)d\tau$$

Lin shows that $\langle v_i(t)v_j(t)\rangle = 2\int_o^t (t-2)\, A_{ij}(\tau)d\tau$ subject to

$$v_i(o) = 0 \quad \text{and} \quad \langle v_i(o)v_j(o) = 0$$

the final equation becomes

$$\frac{d^2}{dt^2}\langle Y_i(t)\; Y_i(t)\rangle = 4t\int_o^t A_{ij}(\tau)\, d\tau - 2\int_o^t \tau\, A_{ij}(\tau)d\tau$$

with τ_1 defined by

$$\int_o^t A_{ij}(\tau)d\tau = \int_o^{t_1} A_{ij}(\tau)d\tau \text{ for all } t > \tau_1$$

τ_2 by

$$\int_{\tau_1}^t A_{ij}(\tau)d\tau \ll \int_o^{\tau_1} A_{ij}(\tau)d\tau \quad \text{for } \tau_1 < t < \tau_2$$

with τ_2 chosen as large as possible and τ_1 as small as possible

τ_3 by

$$\tau_3 = \frac{\int_o^{\tau_1} \tau\, A_{ij}(\tau)d\tau}{\int_o^{\tau_1} A_{ij}\, \tau\, d\tau} \qquad 0 < \tau_3 < \tau_1 < t < \tau_2$$

and $B_{ij} = \int_o^{\tau_1} A_{ij}(\tau)d\tau$

The equations are expressed

$$\frac{d}{dt}\langle v_i v_j \rangle = 2\, B_{ij}$$

$$\frac{d^2}{dt^2}\langle Y_i Y_j \rangle = 4\, B_{ij}\, t - 2\, \tau_3\, B_{ij}$$

and the final form given by Lin $(t \gg \tau_3)$

$$V_{ij} = \langle v_i v_j \rangle = 2\, B_{ij} t$$

$$D_{ij} = \tfrac{1}{2} \frac{d\overline{x}_{ij}}{dz} = B_{ij}\, t^2$$

$$\overline{x_{ij}} = \langle Y_i Y_j \rangle = 2/3\, B_{ij}\, t^3$$

II. DIFFUSION IN SHEAR FLOW

A prediction for the spectral law of energy and the spectral law of shear in the inertial range has been given by C. M. Tchen.[24] He subsequently utilized these predictions to derive relative diffusion laws,[25] introducing a generalized expression for the transfer function W_k (W_k is the fourier transform of the $u_i u_j \frac{\partial u_i}{\partial x_j}$ inertia term) for which the form of the transfer functions postulated by Heisenberg and Obukov are special cases. In the model Tchen proposed, U_i represents the mean flow and u_i, the fluctuation. A production function ψ_k is defined as the fourier transfer of the shear term $u_i u_j \frac{\partial U_i}{\partial x_j}$; the energy dissipation equation in wave space is represented by

$$\epsilon = 2\nu \int_0^k dk'\, k'^2\, E(k') + W_k + \psi_k$$

assuming statistical equilibrium.

In the case $\frac{\partial U_i}{\partial x_j} = U'$ is large.

Tchen finds

$$2 F_{ij} \sim k^{-1}$$

where $F_{ij}(k)$ is the spectrum of $u_i u_j$,

and the energy spectrum is

$$F \sim (\epsilon \quad U')k^{-1} \quad \text{for large } U'$$

The prediction of relative dispersion associated with the k^{-1} law is

$$\langle y^2 \rangle \sim t^2$$

For the case of U' small he obtains the familiar $k^{-5/3}$ energy spectrum and its associated dispersion law

$$\langle y^2 \rangle \sim t^3$$

III. SIMILARITY THEORY OF TURBULENT DIFFUSION IN A STABLY STRATIFIED ATMOSPHERE

In the case of a stably stratified atmosphere at sufficiently large Reynolds number, Bolgianio[26] has suggested that the equilibrium spectrum be divided into three distinct subranges. The inertial subrange is to have a bouyancy subrange defined at its large scale end. The density variation introduces a term into the turbulent energy conservation equation $g/\hat{\rho}_o \ \overline{\delta p w}$ which contains the covariance of density and the

vertical component of the turbulent velocity. A positive value for this covariance indicates turbulent kinetic energy is being converted into potential energy by the turbulence working against gravity. The rate of production of mean square density fluctuations $\chi_{\hat{\rho}}$ is

$$\chi_{\hat{\rho}} = \overline{\delta\rho w} \frac{\overline{\partial\hat{\rho}}}{\partial z}$$

In wave number space $\underline{k}$, the real part of

$$\Phi_{z\rho}\ (\underline{k})$$

where

$$\overline{\delta\rho w} = \int_{k\ \text{space}} \text{Re}\ \left\{\Phi_{z\hat{\rho}}\ (\underset{\sim}{k}')\right\}\ d\underset{\sim}{k}'$$

is a measure of the heat flux contribution at wave number $\underline{k}$. The assumption is made that the co-spectra remains positive in that region where the uniqueness of the vertical direction favors an anisotropic structure. The net result of this energy extraction process is that viscous dissipation may be significantly less than the rate of generation of turbulent energy with the difference representing work against bouyancy. The modification of the inertial subrange of the Kolmogorov theory introduced by the anisotropy associated with the bouyancy affects only the inertial sub-range spectra. The viscosity cutoff $k_d = (\epsilon/\nu^3)^{\frac{1}{4}}$

still divides the usual inertial subrange $E(\underset{\sim}{k}) \sim k^{-5/3}$ from dissipation range of wave numbers. The inertial subrange is divided at wave number k_B

$$k_B = \chi_\rho^{3/4}(g/\rho_o)^{3/2}\ \epsilon^{-5/4}$$

with $k_d > k > k_B$ in the inertial subrange and $k_B \gg k \gg k_1$ in the bouyancy subrange where the "rate of inertial transfer of turbulent energy across the spectrum is much in excess of ϵ" and the local dissipation is small. The removal and insertion of energy into this range proceed at the same rate, however the removal is caused by the working of the vertical turbulent fluctuations against gravity. The parameters which now describe the external effects are no longer ν and ϵ but $\chi_{\hat{\rho}}$ and $g/\hat{\rho}_o$. An energy spectra function summed over all directions in wave number space is predicted to take the form

$$E(k) \sim \chi_\rho^{2/5}(g/\rho_o)^{4/5}\ k^{-11/5}$$

The density fluctuation spectrum is similarly predicted

$$\Gamma_\rho(k) \sim \chi_\rho^{4/5}(g/\rho_o)^{-2/5}k^{-7/5}$$

Two further predictions are given by Bolgiano.

The Richardson number $R_i = gL\ \delta\hat{\rho}/\rho_o\ U^2 \sim gk^{-1/2}\Gamma_\rho^{1/2}/\hat{\rho}kE$ is of order unity throughout the interval, and the relative diffusion of two fluid particles separated by a distance r where $k_B \gg \frac{1}{r} \gg k_1$ is predicted to follow a t^5 law

$$\langle r^2 \rangle \sim \chi_\rho (g/\rho_o)^2\ t^5$$

This prediction is of particular interest for the sodium diffusion experiments since the atmosphere from the mesopeak (85 km) upward is stably stratified. The comparison of this prediction to the behavior of sodium vapor trails is uncertain since the component of the relative dispersion tensor to which this prediction corresponds is not clear. The implications that relative diffusion of two particles within the bouyancy subrange should be isotropic seems, intuitively, to be in conflict with the anistropy which produces it.

IV. KRAICHNAN-ROBERTS PREDICTIONS

The final theory of homogeneous turbulence to be considered was proposed by Kraichnan.[8] It represents a systematic analytical attempt to achieve approximate closure of the infinite set of equations that are the mathematical representation of the self-interaction of the turbulent velocity field. Neglecting molecular diffusion, Roberts[7] has applied Kraichnan's method to the problem of turbulent diffusion in statistically homogeneous flows. If ℓ_o = macroscale of turbulence and v_o is a

characteristic root mean square turbulent velocity, the results may be considered in the asymptotic relation of time to ℓ_o/v_o. The evaluation of $Q(\underset{\sim}{x}', t; \underset{\sim}{x}'', s/\underset{\sim}{x}'_o t_o; \underset{\sim}{x}_o'', s_o)$ in time (i.e., $\frac{\partial Q}{\partial t}$) is expressed by an integro-differential equation. For time $t \ll \frac{\ell}{v_o}$ the results are comparable to those of Batchelor. For times $t \gg \frac{\ell}{v_o}$ or in terms of Richardson's distance-neighbor function for separations $r \gg \ell_o$ the separation p.d.f. approaches a Gaussian form. For separations $r \ll \ell_o$ and at high Reynolds numbers, a variable diffusion coefficient $K(r,t)$ is derived. For all but the very short times this diffusion coefficient is found to be dependent on the separation r and the form of the inertial range spectrum $E(k)$. The assumption of a power law for $E(k)$ allows the dispersion to be evaluated.

From the behavior of the relative dispersion $\langle r^2 \rangle$ as a function of t, when the power laws (Kraichnan) $E(k) \sim k^{-3/2}$ and (Kolmogorov) $E(k) \sim k^{-5/3}$ are used, it is evident that this sensitivity might be used to obtain experimental information to check the different assumptions about the structure of the inertial subrange.

For		Roberts predicts
Energy Spectrum	Variable Diffusion Coefficient	Dispersion Law
$E(k)$	$K(r,t)$	$\langle r^2 \rangle$
$E(k) \sim k^{-3/2}$	$K(r) \sim \epsilon^{1/2} r^{3/2} v_o^{-1/2}$	$\langle r^2 \rangle \sim (\epsilon^2 v_o^{-2}) t^4$
$E(k) \sim k^{-5/3}$	$K(r) \sim \epsilon^{2/3} v_o^{-1} r^{5/3}$	$\langle r^2 \rangle \sim (\epsilon^4 v_o^{-6}) t^6$
$E(k) \sim k^{-1}$	$K(r) \sim v_o r$	$\langle r^2 \rangle \sim v_o^2 t^2$

The Richardson-Batchelor forms

$$K(r) \sim \epsilon^{1/3} r^{4/3} \qquad \langle r^2 \rangle \sim \epsilon t^3$$

do not correspond with the predictions of $E(k) \sim k^{5/3}$ since the Kraichnan approximation does not give an inertial range spectrum which agrees with that derived from the similar theory of Kolmogorov.

REFERENCES

1. Manring, E. R., Bedinger, J. F. and Pettit, H. B., "Some Wind Determinations in the Upper Atmosphere Using Artificially Generated Sodium Clouds," J. Geophys. Res. 64, 587-591 (1959).

2. Bedinger, J. F., Manring, E. R. and Ghosh, S. N., "Study of Sodium Vapor Ejected into the Upper Atmosphere," J. Geophys Res. 63, 19-29 (1958).

3. Marmo, F. F., Pressman, J., Manring, E. R. and Aschenbrand, L., "Artificial Electron Clouds-V," Planet. Space Sci. 2, 174-186 (1960).

4. Manring, E. R., Bedinger, J. F. and Knaflich, H., "Some Measurements of Winds and of the Coefficient of Diffusion in the Upper Atmosphere" in Space Research II ed. by van de Hulst, H. C., de Jager, C. and Moore, A. F., New York, Interscience Publishers, Inc. 1107-1124 (1961).

5. Blamont, J. and de Jager, C., "Upper Atmospheric Turbulence Near the 100 km Level," An. Geophys. 17, 134-144 (1961).

6. Batchelor, G. K., "Diffusion in a Field of Homogeneous Turbulence II. The Relative Motion of Particles," Proc. Cambridge Phil. Soc. 48, 345-362 (1952).

7. Roberts, P. H., "Analytical Theory of Turbulent Diffusion," J. Fluid Mech. 11(2), 257-283 (1960).

8. Kraichnan, R. H., "The Closure Problem of Turbulence Theory" in Hydrodynamic Instability, Vol. 13, Proceedings of Symposia in Applied Mathematics, ed. G. Birkhoff, Amer. Math. Soc., Providence (to be published).

9. Batchelor, G. K., The Theory of Homogeneous Turbulence, Cambridge University Press, Cambridge, p. 197 (1959 Students' Edition).

10. _____, "Application of the Similarity Theory of Turbulence to Atmospheric Diffusion," Quart. J. Roy. Meteor. Soc. 76, 133-146 (1950).

11. Kellogg, W. W., " Diffusion of Smoke in the Stratosphere," J. Meteor. 13, 241-250 (1956).

12. Gifford, Jr., F., "Relative Atmospheric Diffusion of Smoke Puffs," J. Meteor. 14, 410-414 (1957).

13. Gifford, F. A., "The Vertical Variation of Atmospheric Eddy Energy Dissipation", J. Atmos. Sci. 19, 205-206 (1962).

14. Townsend, A. A., The Structure of Turbulent Shear Flow, Cambridge University Press, Cambridge, p. 315 (1956).

15. Corrsin, S., "Transactions of Symposium on Fluid Mechanics in the Ionosphere", J. Geophys. Res. 64, 2055 (1959).

16. Schlichting, H., Boundary Layer Theory, Pergamon Press, New York, p. 535 (1955).

17. Slattery, R. E. and Clay, W. G., "Experimental Measure of Turbulent Transition, Motion Statistics and Gross Radial Growth Behind Hypervelocity Objects", Phys. Fluids (1961).

18. Townsend, A. A., "Turbulent Flow in a Stably Stratified Atmosphere", J. Fluid Mech. 3, 361 (1957).

19. Horowitz, R. and LaGow, H. E., "Upper Air Pressure and Density Measurements from 90 to 220 km with the Viking-7 Rocket", J. Geophys. Res. 62(1), 57-78 (March 1957).

20. Ainsworth, J. E., Fox, F. D. and LaGow, H. E., "Measurement of Upper Atmosphere Structure by Means of Pitot-Static Tube", NASA, Tech. Note D-670, Washington (1961).

21. Greenhow, J. S., "Eddy Diffusion and its Effect on Meteor Trails", J. Geophys. Res. 64, 2208-2209 (1959).

22. Blamont, J. E. and Baguette, J. M., "Measures deduites des deformations de six ruages de metaux alcalins formes par fusees dans la naute atmosphere", Ann. de Geophys. 17, 319-337 (1961).

23. Lin, C. C., "On a Theory of Dispersion by Continuous Movements", I, Proc. Natl. Acad. Sci. 46(4), 566-570 (1960), II, Proc. Natl. Acad. Sci. 46(8), 1147-1150 (1960).

24. Tchen, C. M., "Transport Processes as Foundations of the Heisenberg and Obukhov Theories of Turbulence", Phys. Rev. 93(1), 4-14 (1954).

25. Tchen, C. M., "Diffusion of Particles in Turbulent Flow", in Advances in Geophysics, #6, Academic Press, New York 165-173 (1961).

26. Bolgiano, Jr., R., "Turbulent Spectra in a Stably Stratified Atmosphere", J. Geophys. Res. 64(12), 2226-2229 (1959).